AGU PUBLICATIONS

Geophysical Research Letters

RESEARCH LETTER
10.1002/2015GL064047

Key Points:
- Numerical modeling of oblique subduction zones
- Slab folding, slab dip variations, and induced topography segmentation
- Andean topography segmentation related to the slab folding

Supporting Information:
- Text S1 and Table S2
- Figure S4
- Figure S5
- Figure S6
- Movie S3

Correspondence to:
N. G. Cerpa,
nestor.cerpa@geoazur.unice.fr

Citation:
Cerpa, N. G., R. Araya, M. Gerbault, and R. Hassani (2015), Relationship between slab dip and topography segmentation in an oblique subduction zone: Insights from numerical modeling, *Geophys. Res. Lett.*, *42*, 5786–5795, doi:10.1002/2015GL064047.

Received 30 MAR 2015
Accepted 1 JUL 2015
Accepted article online 4 JUL 2015
Published online 22 JUL 2015

Relationship between slab dip and topography segmentation in an oblique subduction zone: Insights from numerical modeling

Nestor G. Cerpa[1], Rodolfo Araya[2], Muriel Gerbault[3], and Riad Hassani[1]

[1]Observatoire de la Côte d'Azur, Géoazur UMR 7329, Université de Nice Sophia Antipolis, CNRS, IRD, Valbonne, France, [2]Departamento de Ingeniería Matemática, Universidad de Concepción, Concepción, Chile, [3]Géosciences Environnement Toulouse, UMR 5563 CNRS, IRD, Université de Toulouse, Observatoire Midi-Pyrénées, Toulouse, France

Abstract Slab dip controls the state of stress in an overriding plate and affects mountain building. Analog and numerical models have shown variations in tectonic regime induced by slab folding over the 660 km depth discontinuity zone in orthogonal convergence. Here using a three-dimensional model of oblique subduction (30°) and accounting for free top surfaces, we show how slab folding generates an along-strike slab dip segmentation, inducing variations in topography of the overriding plate. When the subducting plate begins to curve forward, the elevation height rises inland and varies along the trench from 5 km to 2 km. The Andes are a suitable natural zone to compare our results with because of its linear margin and well-constrained plates kinematics. Thus, we provide a new explanation to the general decrease in elevation from the central to southern Andes, which still remains to be combined with other 3-D mechanisms to explain the actual Andean topography.

1. Introduction

Subduction zones are generally full 3-D systems, and despite advances in 3-D numerical modeling [*Stegman et al.*, 2006; *Capitanio and Faccenda*, 2012; *Rodríguez-González et al.*, 2012; *Schellart and Moresi*, 2013], flaws remain in quantifying the relationship between deep processes and surface deformation in the overriding plate (OP). Analog models help in assessing this relationship [*Chemenda et al.*, 2000; *Espurt et al.*, 2008; *Martinod et al.*, 2013], but the general limitations in geometry and in parametric space challenge the development of such modeling studies.

Many 3-D subduction models are based on the free-subduction hypothesis which sustains the idea of a predominant role of the slab pull and often leads to the extreme point of view in which the overriding plate is neglected. However, the overriding plate does play an important role in subduction dynamics. Observational studies of present-day subduction zones have shown a relationship between the state of stresses in the back-arc region and OP kinematics [*Jarrard*, 1986; *Heuret and Lallemand*, 2005]. Such observations have been reproduced by analog models of kinematically driven plates where advancing OP (displacement toward the trench) generate back-arc compression, whereas fast retreating OP is associated with extension [*Heuret et al.*, 2007]. Moreover, depending on the combination of plate velocities in these models, the subducting plate (SP) displays different shapes (or subduction styles) upon interaction with the 660 km discontinuity. In these models, evolutions of slab geometry and tectonic regime corroborate statistical studies [*Lallemand et al.*, 2005]. Nevertheless, the link between variations in overriding plate tectonic regime and slab dynamics remains poorly constrained.

Two-dimensional numerical models have explored the dynamics of subduction systems driven by plate motions where the subducting plate anchors at 660 km depth. Results from these experiments have shown that within a given range of applied far-field plate motion, the SP is forced to fold [*Gibert et al.*, 2012; *Cerpa et al.*, 2014]. Slab folding generates variations in time of the subduction dip, changing the state of stresses in the overriding plate and consequently also the surface topography. In 2-D models, *Gibert et al.* [2012] and *Cerpa et al.* [2014] showed that periods of low slab dip generate periods of compression in the overriding plate, consistent with observations in natural subduction zones [*Lallemand et al.*, 2005]. In contrast, the OP stretches when the slab sinks before its first contact with the 660 km discontinuity, and during periods of slab rollback.

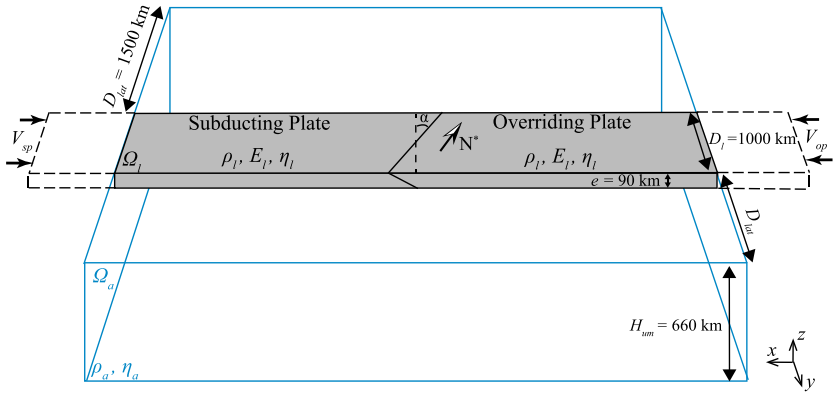

Figure 1. Physical model at initial time. The upper mantle/lower mantle boundary is modeled as an impermeable and frictional barrier. Plate boundary velocities are expressed in reference to this base, with positive v_{op} and v_{sp} corresponding to trenchward motion. We draw an idealized north (N*) for comparison with the Andean margin in the oblique experiment.

While 3-D mantle flow has also been proposed to explain episodic variations in back-arc dynamics in the frame of free-subduction models [*Stegman et al.*, 2006; *Schellart and Moresi*, 2013], here we will not expose the influence of this mantle flow, and it is left for a future contribution.

In the modeling approach used here we make the assumption of a subduction system controlled by plate kinematics so that plates converge toward the trench, a situation representative of about half of the present-day natural subductions zones [*Heuret and Lallemand*, 2005]. Furthermore, we assume a specific trench geometry and a rigid 660 km bottom boundary (as in *Cerpa et al.* [2014]), and we shall test two convergence regimes (orthogonal and oblique) to study the dynamical effects of cyclic slab folding within a 3-D setting.

The goal of the present work is to model a synthetic oblique subduction zone and to relate slab geometries to patterns of vertical deformation in the overriding plate. We first present our numerical method and the model setup. The results are then presented comparing both orthogonal and oblique cases. Finally, we discuss how these results may apply to the Chilean Andes.

2. Mechanical Modeling, Numerical Strategy, and Model Setup

We assume a Maxwell viscoelastic model of plates [*Hassani et al.*, 1997; *Chéry et al.*, 2001] and an isoviscous Newtonian model for the upper mantle. Thermics and chemical transformations are neglected [*Bonnardot et al.*, 2008a] (use similar assumptions in a 2-D approach). We employ a Fictitious Domain Method to resolve the solid-fluid coupling described in *Cerpa et al.* [2014]. Detailed equations are recalled in supporting information Text S1.

Figure 1 displays the geometry of the model setup with complementary mechanical parameters in supporting information Text S1 and Table S2. The two viscoelastic plates are pushed against each other by far-field velocities (v_{op} = 1.5 cm/yr and v_{sp} = 3.0 cm/yr). The plates' lateral boundaries are free slip until they penetrate into the viscous mantle within which they become coupled with the asthenospheric mantle. The plates' top surface remains free. The friction coefficient in between plates is assigned low (μ = 0.015) as in other subudction modeling studies [e.g., *Sobolev and Babeyko*, 2005].

In the fluid, vertical boundaries are open, the bottom base is closed, and the top boundary is free slip. The distance between the plates' lateral vertical boundaries and those of the mantle fluid domain is D_{lat} = 1500 km (D_{lat}/D_l = 1.5) which is evaluated large enough so that boundary effects are negligible [*Schellart and Moresi*, 2013].

An orthogonal subduction (α = 0°) and an oblique subduction (α = 30°) are tested.

Gibert et al. [2012] have determined a kinematic condition that predicts slab folding with 2-D subduction models. If $|v_{op}| < v_s$ ($v_s = v_{op} + v_{sp}$ is the subduction velocity when internal overriding plate deformation is neglected), then the subducting plate folds when depositing over the 660 km discontinuity. This condition is

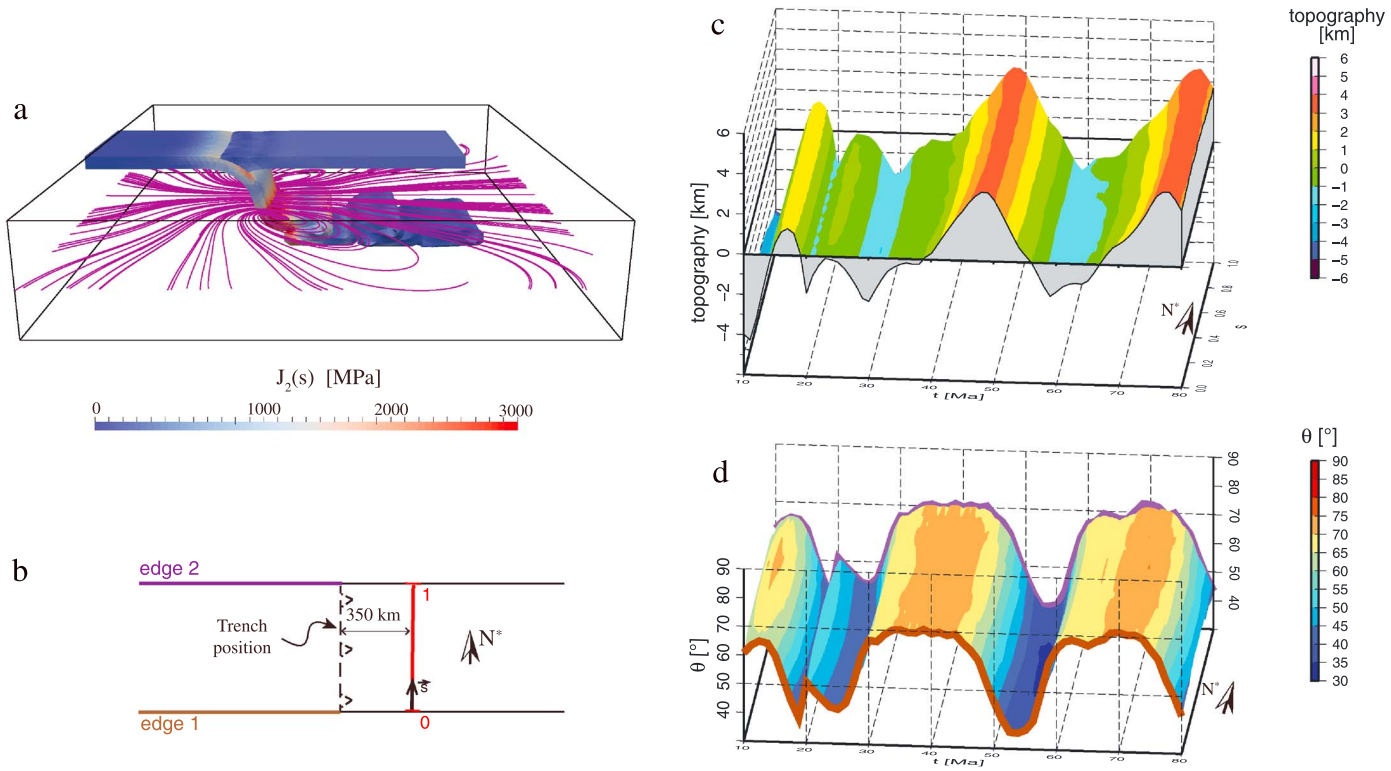

Figure 2. (a) Geometry of plates at final time (circa 85 Ma) in the orthogonal subduction experiment. Blue-to-red color scale displays the second invariant of deviatoric stresses ($J_2(s)$) in plates, and magenta lines define the streamlines of in-plane horizontal mantle flow at 400 km depth. (b) Sketch of the line along which topography is plotted in Figure 2c through time, and of the subducting plate edges for which slab dips are plotted in Figure 2d through time. (c) Evolution of topography versus time at 350 km from the trench. (d) Along-strike variations of slab dip through time, averaged between 150 km and 350 km depth (slab dip at the two edges of the slab are drawn in brown and magenta).

valid in case of a large enough plate/mantle viscosity ratio ($\geq 10^4$ [*Cerpa et al.*, 2014]). Hence, our model setup stands within this range of parameters.

3. Results

3.1. Orthogonal Convergence

We first perform a 3-D orthogonal subduction experiment. The system's final state after circa 85 Ma is displayed in Figure 2a.

Comparison between an equivalent 2-D subduction model (not shown here but similar examples are described in, e.g., *Cerpa et al.* [2014]) and the 3-D orthogonal model shows similar plates dynamics.

After subduction initiation, the slab sinks into the mantle down to the 660 km discontinuity zone. Because of the plates/mantle positive density contrast, the trench retreats, resulting in overriding plate stretching. The first interaction between the slab tip and the impermeable barrier at 660 km depth can produce a fold depending on the slab's dip just before this interaction. Hereafter, we will rather refer to this event as "slab anchoring." Once the slab is anchored it then folds periodically. The present work focuses on plates dynamics after anchoring and on its expression at the top surface.

We distinguish four typical stages during a folding cycle: (1) slab rollback before folding; (2) beginning of folding during which the slab curves forward, i.e., toward the OP; (3) vertical sinking of the fold; and (4) closing of the fold and reinitiation of slab rollback.

As the SP folds over the 660 km depth boundary its dip varies in time, generating variations in stress regime of the OP. These variations generate cyclic vertical displacement of the overriding plate's free surface. We represent in Figure 2c the temporal evolution of topography after slab anchoring and during two slab folding cycles, along a fixed line located 350 km away from the trench (see Figure 2b). Topography varies between a negative low (−3 km) and a positive high (4 km) depending on the folding stage.

Lateral variations in slab dip are displayed through time (Figure 2d). No significant differences appear. There are also negligible variations in plate deformation (i.e., no slab nor trench incurvation) and in topography along strike (in the direction parallel to the trench; Figure 2c). Note that maximum elevation at the top surface is reached during the compressional event that precedes the minimum slab dip.

3.2. Oblique Convergence

We present now the results from the oblique subduction experiment. The general system behavior is similar to that of the orthogonal case. Until the slab tip reaches the impermeable barrier at 660 km depth, the OP stretches. Once the slab is anchored, it folds periodically as in the orthogonal case. The final state is displayed Figure 3a.

During the experiment and because of the obliquity, the slab dip varies along strike. Thus, the stress field and topography in the OP also vary in this direction, as described below.

Figures 3b–3e display the slab dip, the orientation of principal deviatoric stresses at the surface of the OP, and the topography at four moments corresponding to the four stages cited above. We shall rather focus on the description of the tectonic regime and topography far from the trench (>150 km). Closer than 150 km, the OP's surface is complex in detail but remains at first order under compression and subsidence due to the plates' density contrast [*Bonnardot et al.*, 2008b].

During stage 1 characterized by rollback at time 34 Ma (Figure 3b), the slab is nearly vertical and its dip exceeds 70° over a broad width (parallel to axis *y*). The OP is in extension, and little topography is observed. Far from the trench principal stresses are oriented parallel to the plate axis (*x* axis) and their magnitude is low. Seven hundred kilometers inland, stresses progressively rotate subparallel to the trench direction and increase slightly in intensity when approaching the trench. This rotation pattern is similar in the following stages except for stage 3.

At 43 Ma, a slab fold initiates (stage 2, Figure 3c). At this moment the slab curves forward and its dip decreases. Because of the obliquity, folding does not start at the same moment along the margin and thus the slab dip at a given moment varies along strike. Near one lateral boundary of the slab, the dip is lower than 30° up to 200 km depth, whereas at the same moment the other lateral boundary displays a dip close to 50° down to 400 km depth. Folding triggers a compressional event in the overriding plate, and an important topography develops reaching a height of 4–5 km about 200 km wide along the lateral plate boundary and is associated with a shallowly dipping slab. As the slab dip increases to the other end of the plate boundary (e.g., southward), compressional stresses vanish and topography narrows and decreases to a height of 2 km.

After forward slab incurvation, the slab sinks again vertically (stage 3). We represent this stage at 45 Ma (Figure 3d). The obliquity generates a delay in this sinking along the margin, and thus, another segmentation of the slab dip occurs. Vertical sinking generates in the OP a tensile stress regime parallel to the plate axis, and the positive topography built in the previous stage disappears. The highest relief shifts inland to about 700 km and reduces down to an amplitude of about 1 km.

The folding cycle ends around 53 Ma when the fold closes over itself and the slab starts to rollback again (stage 4, Figure 3e). The slab dip increases (>70°) and becomes more homogeneous along strike. During this period, no significant topography develops in the overriding plate since it is subjected to a tensile regime of greater intensity compared to previous moments (300 MPa at 500–600 km away from the trench).

Figure 4b displays the temporal evolution of topography, 350 km inland from the trench (see Figure 4a). After slab anchoring, the topography varies between a negative low (−3 km) and a positive high (2–5 km) depending on the folding stage. Two stages of high elevation correspond to two episodes of slab folding at about 25 Myr interval. This elevation exceeds 5 km along one lateral boundary, whereas it reaches only 2 km along the other boundary at the same moment.

We display in Figure 2c along-strike temporal variations in dip angle. Along one edge the slab dip varies from 30° to 70°, whereas along the other end it varies only from 40° to 60°. The edge with the greatest variation in slab dip coincides with the lowest dip and highest topography during folding. Most important, the slab dip reaches its minimum values at both slab edges with a delay of about 8 Ma one with the other, and this means that during folding there will be a segmentation of the subduction angle along strike. Therefore, maximum topography is not achieved simultaneously (Figure 4b) along the arc region parallel to the trench.

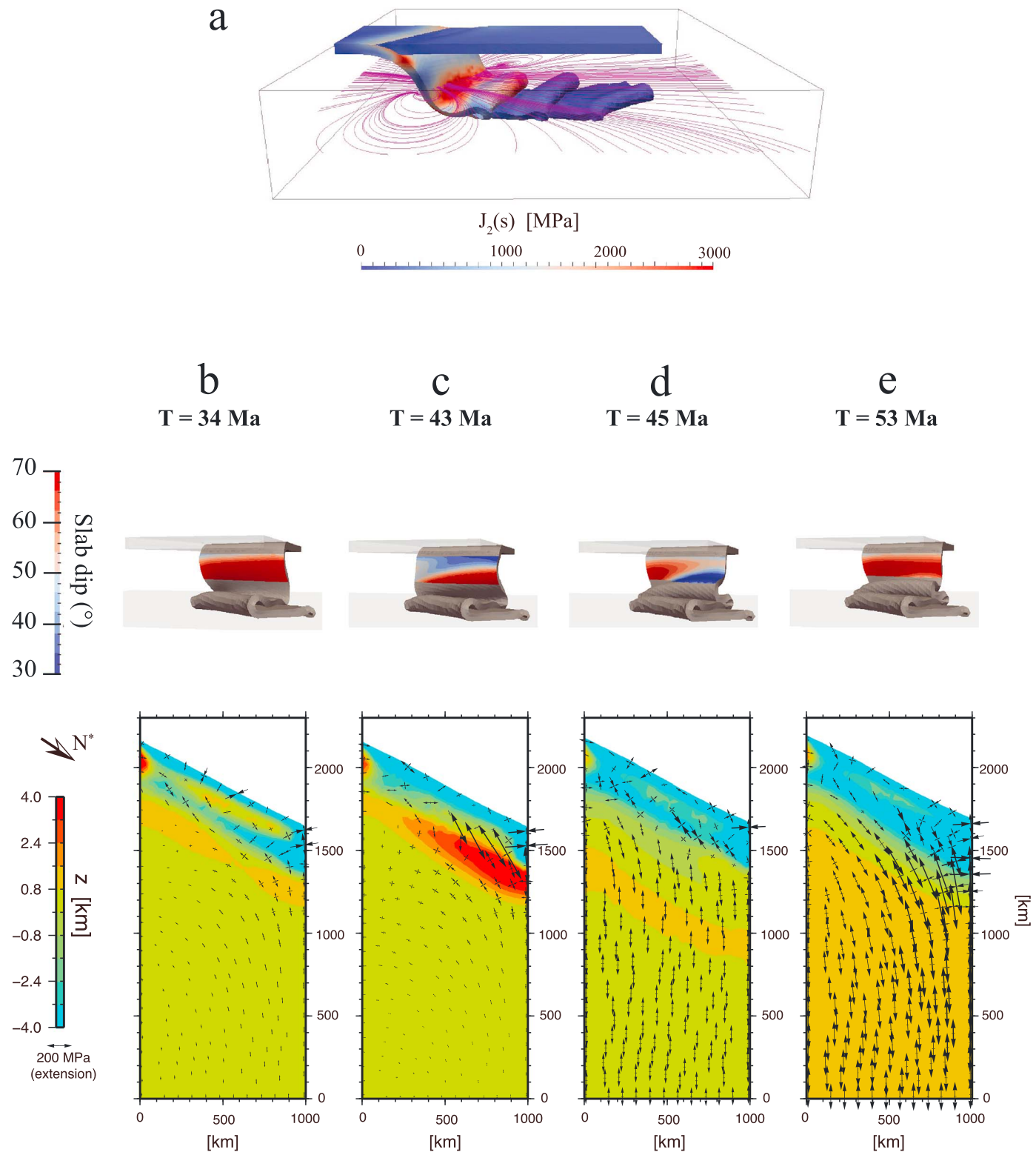

Figure 3. (a) Geometry of plates at final time (circa 85 Ma) for the oblique subduction experience. Color scales same as Figure 2a see corresponding figure caption. (b–e) (top) Geometry of plates and slab dip (displayed only for depths between 120 and 400 km). (bottom) Topography (color scale) and crosses of the principal deviatoric stresses at the surface of the OP, indicating their direction and amplitude.

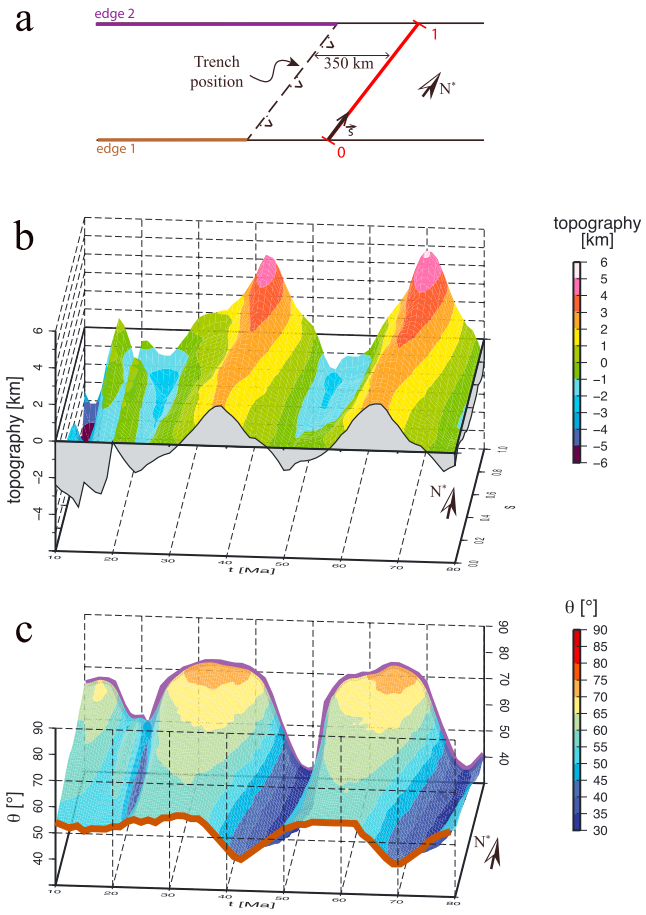

Figure 4. (a) Sketch of the line along which topography is plotted. (b and c) The same as Figures 2c and 2d.

4. Modeling Discussion

In the models presented here, we assumed a rigid barrier at 660 km depth. This forced stagnation is a process supported by tomographic images in several subduction zones [*Fukao and Obayashi*, 2013]. It appears as a transitional stage before further slab sinking into the lower mantle and may be a common behavior of natural subduction systems [*Fukao and Obayashi*, 2013]. An interesting future study would be to test a similar setup in which the slab could penetrate into the lower mantle. Cyclic slab folding could then turn into slab buckling within the transition zone as predicted by semianalytic solutions [*Ribe et al.*, 2007] and 2-D numerical models [*Lee and King*, 2011; *Čížková and Bina*, 2013].

The assumption of kinematically driven plates, as in previous work [*Gibert et al.*, 2012; *Cerpa et al.*, 2014], is also strong. It is found pertinent in subduction zones like the Andes involving a young subducting plate which is close to neutral buoyancy, and thus for which the slab pull cannot be the dominant driving force.

Three-dimensional models of orthogonal free subduction [e.g., *Schellart*, 2004; *Morra and Regenauer-Lieb*, 2006] have evidenced variations in slab deformation in the direction parallel to the trench (i.e., slab incurvation), in relation to toroidal mantle flow around its edges. We do not observe this feature in our models, and instead, our slab dips and stress field in the OP remain constant along strike. We attribute this homogeneity to the presence of the OP as well as to assumptions of a high-viscosity ratio and a moderate width of plates, in contrast to other studies. Because of the similarities of our 3-D orthogonal experiment and 2-D experiments, we conclude that a 2-D plane-strain approach is suitable in such a context.

In the present contribution the novelty consists in accounting for oblique convergence, which generates an along-strike slab dip segmentation, in time and space while the slab folds. On one hand, the folding mechanism generates cyclic variations in time of the stress field of the OP similar to the orthogonal setting. On the other hand, the spatial rotation of stresses results from the obliquity of the subducting plate, since it is

also obtained in an alternative model without slab folding (cf. additional model Figure S5). The combination of both the folding process and the oblique convergence generates cyclic along-strike variations in slab dip that enhance alternating periods of tensile and compressional stress regimes in the OP, at different moments along the plate margin.

The difference in slab dip between both edges of the slab (see Figure 4c) reflects a delay in the development of folds. At the surface, these folding periods are linked to a maximum elevation (which precedes in time the minimum slab dip), which therefore does not occur at the same moment along the trench-parallel direction (delay of 10–15 Ma).

When the slab dip decreases during the onset of folding, our model shows maximum elevations in the overriding plate varying from about 2 km to more than 4 km from one edge to the other. However, we note that the highest elevation is reached above the location where the slab folds over an already deposited portion of slab. In contrast, the fold below the region of lowest elevation deposits directly over the 660 km discontinuity. Thus, slab dip amplitude may increase (or decrease) due to this geometrical feature and thus may also enhance the segmentation of topography at identical moments along the margin.

We recall briefly how variations in folding periodicity and stress regime are sensitive to several parameters [e.g., *Gibert et al.*, 2012, and references therein]: Weaker plates produce steeper slab dips and thus less compression in the overriding plate; if the subducting rate increases or the overriding plate velocity decreases, then the spacing between two folds decreases; and a relatively lighter (e.g., younger) plate is predicted to decrease its subducting dip and thus increases (and/or broadens) OP compression.

Finally, we recall that the absolute intensity of stresses (and thus mountain building) also depends on interplate friction, on plates strength, and on irreversible (e.g., plastic) deformation [e.g., *Gerbault et al.*, 2009; *Capitanio et al.*, 2011, and references therein], parameters that remain to be analyzed in 3-D slab folding models.

5. Geodynamic Application to the Andes

The Andes is the greatest orogenic system related to the subduction of an oceanic plate and extends over 8000 km. Although the Cordillera is continuous along the South American margin, it presents latitudinal variations in topography, geology, and volcanism related to its complex history [e.g., *Ramos*, 2009]. Little variations in plate kinematics in the last 50 Ma [e.g., *Somoza and Ghidella*, 2012] make the Andes an ideal natural oblique subduction zone to study by the means of numerical modeling. Plate kinematics reconstructions for the Andes since the Late Cretaceous [*Pardo-Casas and Molnar*, 1987; *Somoza and Ghidella*, 2012] indicate a stable obliquity of 20–25° since 35 Ma, from North (22°S) to South (40°S) Chile [see *Haschke et al.*, 2006, and references therein]. In contrast before in the Eocene (34–50 Ma), the obliquity was about 40°at the same locations. Therefore, the obliquity angle of 30° assumed in our oblique model appears comparable to the Chilean Andes.

However, we note that (1) our models have lower imposed convergence velocity than estimates for the Andes during the Cenozoic [*Pardo-Casas and Molnar*, 1987; *Somoza and Ghidella*, 2012] and that (2) our modeled plate width is relatively narrow (1000 km). These discrepancies rise from limitations in computational time. Yet as an answer to issue (1), *Gibert et al.* [2012] demonstrated that a faster convergence rate of the overriding plate increases its compressional state and decreases the period in between two folding events. And in answer to issue (2), alternative 3-D models not presented here show that increasing plates width mainly increases the time delay in between slab dip variations along strike.

In our oblique model, the principal stresses displayed in Figure 3 show stress partitioning in the overriding plate, with a broad region displaying increasing values and rotating directions of the maximum shear stress. We expect this shear component to be accommodated by long-term nearly trench-parallel permanent structures in nature, and this is indeed the case of the Liquiñe–Ofqui Fault Zone in the Southern Andes and the Atacama fault zone in Northern Chile [*Cembrano et al.*, 2007].

The general extension observed inland in our experiments differs from observations in the Andes. However, cyclic periods of compression lasting for about 25 Myr were obtained, and in the Andes, periods of orogenic building since 100 Ma were not under a constant regime either [e.g., *Ramos*, 2009]. The aim of the present paper not being to fit exactly the Andes but rather to discuss relative tendencies, we did not seek for most

appropriate initial conditions. Yet the evolution of topography 300–400 km inland may be compared with the Andes as follows.

Along the straight margin segment of the central Andes from 18°S to 30°S southward, the mountain belt today displays a constant average height of 5 km, but its width diminishes. Along this 1000 km portion of the plate margin, the slab dip decreases from 30° beneath southern Peru to less than 20° southward [*Isacks*, 1988]. Our results are in contradiction with these observations, since our model generates an increasing slab dip and a decreasing topography from north to south. Therefore, factors other than oblique convergence must control mountain building in this area (cf. next paragraph). If we now consider the 1000 km long plate margin farther south from 33.5°S down to ~43°S, surface elevation continues to decrease down to an average of 2 km [*Ramos*, 2005], while the slab dip steepens. This observation is now consistent with our model results, suggesting a role of convergence obliquity. In turn, variations in eastward arc expansion, discontinuous extensional basins, and volcanism may be linked with temporal variations in slab dip within the last 100 Myr [*Folguera and Ramos*, 2011] and thus may reflect slab folding.

The Andean margin is characterized by two flat slabs, the Nazca ridge around 15°S in Peru and the Juan Fernandez ridge around 33°S in Chile. The subduction of buoyant oceanic ridges is now well identified as being able to cause horizontal subduction [*Gutscher et al.*, 2000; *Van Hunen et al.*, 2002] and increased uplift in the overriding plate [e.g., *Espurt et al.*, 2008]. Analog models indicate elevations up to approximately 7 km during the horizontal subduction of a ridge 250 km large, which was compared to the effect of the Nazca ridge [*Martinod et al.*, 2013]. However, the buoyancy of the Juan Fernandez ridge remains problematic [*Marot et al.*, 2014], and in a more general frame view, horizontal subduction can also result from other factors [*Van Hunen et al.*, 2002; *Haschke et al.*, 2006; *Gerbault et al.*, 2009; *O'Driscoll et al.*, 2012; *Skinner and Clayton*, 2013; *Cerpa et al.*, 2014].

On the other hand, periods of enhanced compression or extension along the Chilean margin cannot be solely explained by the subduction of oceanic ridges [*Cembrano et al.*, 2007], although variations in subduction dip are invoked [*Ramos*, 2009; *Folguera and Ramos*, 2011]. Therefore, the segmentation modeled here with slab folding may explain such alternations. Unfortunately, tomographic data imaging the behavior of the Nazca plate in the mantle transition zone still lack resolution to prove this [e.g., *Fukao and Obayashi*, 2013; *Scire et al.*, 2014].

Along strike variations in shortening and mountain height throughout the Andes are also attributed to climatic and rheological variations. A dry climate in the north maintains high interplate friction and high topography, whereas the humid conditions in the south lubricate the plate interface and diminish gravity counterbalance [*Lamb and Davis*, 2003]. Variations in internal strength of the oceanic plate and of the accreted terranes composing the South American plate also explain variations in amounts of shortening [e.g., *Gerbault et al.*, 2009; *Capitanio et al.*, 2011]. In our models we have assumed a homogeneous intraplate friction and homogeneous viscoelastic plates. A numerical study accounting for all the involved parameters in 3-D remains to be conducted in order to decipher these effects.

6. Summary and Conclusion

With a 3-D mechanical approach we have obtained a process of oblique subduction that could partially explain the segmentation of topography along the Andes. Since compression events in the overriding plate are due to the slab dip evolution, the results point to a strong relationship between along-strike variations in slab dip and variations in elevation of the overriding plate. The model also displays deformation partitioning, occurring in the arc area along the plate margin.

Amongst the perspectives regarding modeling of oblique subduction, accounting for variable interplate friction and for brittle-plastic behavior will allow to study the localization of deformation and its cumulated effects over time. Temperature-dependent rheologies, surface processes, and a permeable transition zone shall also help in better characterizing the long-term evolution of the Andes. A retroaction of internal driving forces onto plate boundary motion [e.g., *Quinteros and Sobolev*, 2013] deserves to be explored further in 3-D. Effects of mantle viscosity [e.g., *Cerpa et al.*, 2014], particularly when the plates are large [*Schellart et al.*, 2007], also remain to be studied.

Acknowledgments
This work was granted access to the HPC and visualization resources of the "Centre de Calcul Interactif" hosted by the "Université Nice Sophia Antipolis." It was supported by a grant from "ECOS-Sud Chili-France" (action C13U03). All data, parameters, and methods needed for understanding and replicating this work are presented in the manuscript. The two anonymous reviewers are thanked for their detailed and constructive comments.

The Editor thanks two anonymous reviewers for their assistance in evaluating this paper.

References

Bonnardot, M.-A., R. Hassani, and E. Tric (2008a), Numerical modelling of lithosphere-asthenosphere interaction in a subduction zone, *Earth Planet. Sci. Lett.*, *272*(3–4), 698–708, doi:10.1016/j.epsl.2008.06.009.

Bonnardot, M.-A., R. Hassani, E. Tric, E. Ruellan, and M. Régnier (2008b), Effect of margin curvature on plate deformation in a 3-D numerical model of subduction zones, *Geophys. J. Int.*, *173*(3), 1084–1094.

Capitanio, F., and M. Faccenda (2012), Complex mantle flow around heterogeneous subducting oceanic plates, *Earth Planet. Sci. Lett.*, *353*, 29–37.

Capitanio, F., C. Faccenna, S. Zlotnik, and D. Stegman (2011), Subduction dynamics and the origin of the Andean orogeny and the Bolivian orocline, *Nature*, *480*, 82–86.

Cembrano, J., A. Lavenu, G. Yañez, R. Riquelme, M. García, G. González, and G. Hérail (2007), Neotectonics, in *The Geology of Chile*, edited by T. Moreno and W. Gibbons, pp. 231–261, The Geol. Soc., London, U. K.

Cerpa, N. G., R. Hassani, M. Gerbault, and J.-H. Prévost (2014), A fictitious domain method for lithosphere-asthenosphere interaction: Application to periodic slab folding in the upper mantle, *Geochem. Geophys. Geosyst.*, *15*, 1852–1877, doi:10.1002/2014GC005241.

Chemenda, A., S. Lallemand, and A. Bokun (2000), Strain partitioning and interplate friction in oblique subduction zones: Constraints provided by experimental modeling, *J. Geophys. Res.*, *105*(B3), 5567–5581.

Chéry, J., M. D. Zoback, and R. Hassani (2001), An integrated mechanical model of the San Andreas fault in Central and Northern California, *J. Geophys. Res.*, *106*(B10), 22,051–22,066, doi:10.1029/2001JB000382.

Čížková, H., and C. Bina (2013), Effects of mantle and subduction-interface rheologies on slab stagnation and trench rollback, *Earth Planet. Sci. Lett.*, *379*, 95–103.

Espurt, N., F. Funiciello, J. Martinod, B. Guillaume, V. Regard, C. Faccenna, and S. Brusset (2008), Flat subduction dynamics and deformation of the South American plate: Insights from analog modeling, *Tectonics*, *27*, TC3011, doi:10.1029/2007TC002175.

Folguera, A., and V. A. Ramos (2011), Repeated eastward shifts of arc magmatism in the southern Andes: A revision to the long-term pattern of Andean uplift and magmatism, *J. South Am. Earth Sci.*, *32*(4), 531–546.

Fukao, Y., and M. Obayashi (2013), Subducted slabs stagnant above, penetrating through, and trapped below the 660 km discontinuity, *J. Geophys. Res. Solid Earth*, *118*(11), 5920–5938, doi:10.1002/2013JB010466.

Gerbault, M., J. Cembrano, C. Mpodozis, M. Farias, and M. Pardo (2009), Continental margin deformation along the Andean subduction zone: Thermo-mechanical models, *Phys. Earth Planet. Int.*, *177*(3), 180–205.

Gibert, G., M. Gerbault, R. Hassani, and E. Tric (2012), Dependency of slab geometry on absolute velocities and conditions for cyclicity: Insights from numerical modelling, *Geophys. J. Int.*, *189*(2), 747–760, doi:10.1111/j.1365-246X.2012.05426.x.

Gutscher, M.-A., W. Spakman, H. Bijwaard, and E. Engdahl (2000), Geodynamics of flat subduction: Seismicity and tomographic constraints from the Andean margin, *Tectonics*, *19*(5), 814–833.

Haschke, M., A. Günther, D. Melnick, H. Echtler, K.-J. Reutter, E. Scheuber, and O. Oncken (2006), Central and Southern Andean tectonic evolution inferred from arc magmatism, in *The Andes*, pp. 337–353, Springer, Berlin.

Hassani, R., D. Jongmans, and J. Chéry (1997), Study of plate deformation and stress in subduction processes using two-dimensional numerical models, *J. Geophys. Res.*, *102*(B8), 17,951–17,965, doi:10.1029/97JB01354.

Heuret, A., and S. Lallemand (2005), Plate motions, slab dynamics and back-arc deformation, *Phys. Earth Planet. Int.*, *149*(1), 31–51.

Heuret, A., F. Funiciello, C. Faccenna, and S. Lallemand (2007), Plate kinematics, slab shape and back-arc stress: A comparison between laboratory models and current subduction zones, *Earth Planet. Sci. Lett.*, *256*(3), 473–483.

Isacks, B. L. (1988), Uplift of the central Andean plateau and bending of the Bolivian orocline, *J. Geophys. Res.*, *93*(B4), 3211–3231.

Jarrard, R. D. (1986), Relations among subduction parameters, *Rev. Geophys.*, *24*(2), 217–284.

Lallemand, S., A. Heuret, and D. Boutelier (2005), On the relationships between slab dip, back-arc stress, upper plate absolute motion, and crustal nature in subduction zones, *Geochem. Geophys. Geosyst.*, *6*, Q09006, doi:10.1029/2005GC000917.

Lamb, S., and P. Davis (2003), Cenozoic climate change as a possible cause for the rise of the Andes, *Nature*, *425*(6960), 792–797.

Lee, C., and S. D. King (2011), Dynamic buckling of subducting slabs reconciles geological and geophysical observations, *Earth Planet. Sci. Lett.*, *312*(3), 360–370.

Marot, M., T. Monfret, M. Gerbault, G. Nolet, G. Ranalli, and M. Pardo (2014), Flat versus normal subduction zones: A comparison based on 3-d regional traveltime tomography and petrological modelling of Central Chile and Western Argentina (29°-35°s), *Geophys. J. Int.*, *199*(3), 1633–1654.

Martinod, J., B. Guillaume, N. Espurt, C. Faccenna, F. Funiciello, and V. Regard (2013), Effect of aseismic ridge subduction on slab geometry and overriding plate deformation: Insights from analogue modeling, *Tectonophysics*, *588*, 39–55, doi:10.1016/j.tecto.2012.12.010.

Morra, G., and K. Regenauer-Lieb (2006), A coupled solid-fluid method for modelling subduction, *Philos. Mag.*, *86*(21–22), 3307–3323.

O'Driscoll, L. J., M. A. Richards, and E. D. Humphreys (2012), Nazca-South America interactions and the late Eocene-late Oligocene flat-slab episode in the Central Andes, *Tectonics*, *31*, TC2013, doi:10.1029/2011TC003036.

Pardo-Casas, F., and P. Molnar (1987), Relative motion of the Nazca (Farallon) and South American plates since late cretaceous time, *Tectonics*, *6*(3), 233–248.

Quinteros, J., and S. Sobolev (2013), Why has the Nazca plate slowed since the Neogene?, *Geology*, *41*(1), 31–34.

Ramos, V. A. (2005), Seismic ridge subduction and topography: Foreland deformation in the Patagonian Andes, *Tectonophysics*, *399*(1), 73–86, doi:10.1016/j.tecto.2004.12.016.

Ramos, V. A. (2009), Anatomy and global context of the Andes: Main geologic features and the Andean orogenic cycle, in *Backbone of the Americas: Shallow Subduction, Plateau Uplift, and Ridge and Terrane Colli, Mem. Geol. Soc. Am., 204*, pp. 31–65.

Ribe, N. M., E. Stutzmann, Y. Ren, and R. Van Der Hilst (2007), Buckling instabilities of subducted lithosphere beneath the transition zone, *Earth Planet. Sci. Lett.*, *254*(1), 173–179.

Rodríguez-González, J., A. Negredo, and M. Billen (2012), The role of the overriding plate thermal state on slab dip variability and on the occurrence of flat subduction, *Geochem. Geophys. Geosyst.*, *13*, Q01002, doi:10.1029/2011GC003859.

Schellart, W. (2004), Kinematics of subduction and subduction-induced flow in the upper mantle, *J. Geophys. Res.*, *109*, B07401, doi:10.1029/2004JB002970.

Schellart, W., J. Freeman, D. Stegman, L. Moresi, and D. May (2007), Evolution and diversity of subduction zones controlled by slab width, *Nature*, *446*(7133), 308–311.

Schellart, W. P., and L. Moresi (2013), A new driving mechanism for backarc extension and backarc shortening through slab sinking induced toroidal and poloidal mantle flow: Results from dynamic subduction models with an overriding plate, *J. Geophys. Res. Solid Earth*, *118*(6), 3221–3248, doi:10.1002/jgrb.50173.

Scire, A., C. Biryol, G. Zandt, and S. Beck (2014), Imaging the Nazca slab and surrounding mantle to 700 km depth beneath the central Andes (18°S to 28°S), in *Geodynamics of a Cordilleran Orogenic System*, vol. 212, pp. 23–41, Geol. Soc. of Am. Memoirs, The Central Andes of Argentina and Northern Chile.

Skinner, S. M., and R. W. Clayton (2013), The lack of correlation between flat slabs and bathymetric impactors in South America, *Earth Planet. Sci. Lett.*, *371*, 1–5.

Sobolev, S. V., and A. Y. Babeyko (2005), What drives orogeny in the Andes?, *Geology*, *33*(8), 617–620.

Somoza, R., and M. E. Ghidella (2012), Late Cretaceous to recent plate motions in western South America revisited, *Earth Planet. Sci. Lett.*, *331*, 152–163.

Stegman, D. R., J. Freeman, W. P. Schellart, L. Moresi, and D. May (2006), Influence of trench width on subduction hinge retreat rates in 3-D models of slab rollback, *Geochem. Geophys. Geosyst.*, *7*, Q03012, doi:10.1029/2005GC001056.

Van Hunen, J., A. Van Den Berg, and N. Vlaar (2002), On the role of subducting oceanic plateaus in the development of shallow flat subduction, *Tectonophysics*, *352*(3), 317–333.